Simulation of temperature influence on flow pattern and residence time in a detention tank

Åsa Adamsson and Lars Bergdahl*

Water Environment Transport, Chalmers University of Technology, SE-412 96 Göteborg, Sweden. *Corresponding author. E-mail: *lars.bergdahl@wet.chalmers.se*

Received 23 August 2004; accepted in revised form 8 April 2005

Abstract Three-dimensional simulations were used to model how a temperature difference between the incoming water and tank water influences the flow pattern and residence time in a detention tank. Buoyant, neutrally buoyant and negatively buoyant incoming jets were simulated. The simulations were compared with measurements for neutrally buoyant jets in a large-scale model of a detention tank (13 × 9 × 1 m). The results show that a negatively buoyant jet gives slightly less effective volume, defined as the time when 50% of added tracer has passed the outlet divided by the nominal residence time, than a neutrally buoyant jet. The flow pattern for a negatively buoyant jet at low densimetric Froude numbers consists of a current that travels along the bottom towards the outlet and a counter current at the surface towards the inlet, while the neutrally buoyant jet excites a surface jet with two large eddies on each side of the jet. This implies that the short-circuiting will decrease when a negatively buoyant jet at low densimetric Froude number occurs in the tank. The difference between the flow pattern excited by a buoyant jet and a neutrally buoyant jet is small.

Keywords Computational fluid dynamics; detention tank; negatively buoyant jets; residence time; stormwater; temperature

Notation

Roman letters

a_0–a_5	constants in the water density equation
$C_{\varepsilon 1}$	constant 1.44, in the k–ε turbulence model
$C_{\varepsilon 2}$	constant 1.92, in the k–ε turbulence model
C_μ	constant 0.09, in the k–ε turbulence model
c	effluent tracer concentration
c_p	specific heat
c_0	initial mass of tracer divided by volume of the tank
D_m	molecular diffusion coefficient
d	pipe diameter
e	measure of effective volume
F_0	densimetric Froude number
g_i	acceleration due to gravity
K	thermal conductivity
k	turbulent kinetic energy
m	local mass fraction of tracer
P	average pressure
S	measure of short-circuiting
S_{ct}	turbulent Schmidt number
S_{ji}	mean strain rate tensor

Nordic Hydrology **Vol 37 No 1 pp 53–68** © IWA Publishing 2006

doi: 10.2166/nh.2005.030

T	temperature
T_{in}	influent water temperature
T_{tank}	tank water temperature
t	time
t_n	nominal residence time
t_{16}, t_{50}	time at which 16%, 50% of the tracer has passed the outlet
U_i	average velocity in the x, y and z directions
u'_i	fluctuating velocity in the x, y and z directions
x_i	coordinate

Greek letters

β	thermal expansion coefficient
ε	dissipation rate of k
μ	molecular dynamic viscosity
μ_t	turbulent dynamic viscosity
ρ	density of water
ρ_{in}	inflow water density
ρ_{tank}	ambient (tank) water density
σ_ε	constant 1.3, in the $k-\varepsilon$ turbulence model
σ_k	constant 1.0, in the $k-\varepsilon$ turbulence model
σ_t	turbulent Prandtl number

Introduction

The design of stormwater ponds is currently based primarily on the assumption that plug flow conditions prevail in the pond and that 100% of the pond volume is used. This is not the case for most ponds, as the flow structure is normally composed of zones of recirculation and eddies. Plug-like flow conditions are only attained in ponds with large length-to-width ratios (Persson 2000). In the future, general design procedures are needed that can predict optimal function from given hydrologic, hydraulic and topographic conditions for stormwater ponds, wetlands and detention tanks.

The shape of the pond should be the result of balancing between hydrodynamics (flow pattern and velocity), aesthetic factors and maintenance aspects. Several factors affect the hydrodynamics of a pond. German *et al.* (2003) suggested a division into four major categories: upstream boundary conditions, pond shape, downstream boundary conditions and meteorological conditions.

Several studies can be found in the literature that deal with pond shape and layout to receive an optimal shape (Hvitved-Jacobsen *et al.* 1994; Walker 1998; Larm 2000; Persson 2000; German 2003). Although an optimal shape is obtained, changes in upstream boundary conditions, i.e. inflow characteristics such as flow rate, pollutants, salt and temperature, or local meteorological conditions, e.g. precipitation, wind (Marsalek *et al.* 2003; German *et al.* 2003) and temperature, may affect the performance of the pond and give rise to different flow phenomena, e.g. eddies, recirculations, short-circuiting currents and stratification.

Stratification depends mainly on inflow characteristics and local meteorological conditions and can be caused by differences in density between the jet and the ambient fluid. Density differences caused by particles or sludge concentration can, for the most part, be neglected for stormwater ponds, since the concentration of particles is low. Stratification caused by differences in temperature and salinity is more likely.

Temperature differences in stormwater ponds can, for example, occur during the summer months when the water in the pond is warmed by the sun. Few studies have been found of temperature influence on stormwater ponds in warm climates or in summer. One, however, is

Van Buren *et al.* (2000), who made temperature measurements in the Kingston stormwater pond from July to September and found temperature differences in the vertical plane. After a period of prolonged low flow, dry antecedent condition and calm winds, the average temperature at the surface was 3.6°C higher than the average temperature at the bottom.

The performance of stormwater ponds is affected in many ways in winter conditions. An ice layer may form, which decreases the influence of wind on the flow (Marsalek *et al.* 2003), and thermal stratification may more easily evolve. In the spring, the melt water carries pollutants that have accumulated during the winter period (Oberts *et al.* 2000). This melt water may have high levels of salinity, often associated with road salting, which reduces settling velocity and oxygen levels. The result is less settling of particles and possibly the release of metals from the sediment (Oberts 1994). The high levels of salinity also affect the density and may cause chemical stratification. Pettersson (1999) made extensive measurements in a stormwater pond in Göteborg, Sweden, that showed a high conductivity during snowmelt events, which indicated high salinity. Marsalek *et al.* (2000, 2003) studied the Kingston stormwater pond under winter operation. The flow patterns were found to be complex and affected by density stratification. While chemical stratification was dominant, thermal stratification was also observed. They concluded that a buoyant jet occurs in winter when water with a low amount of total dissolved solids or a temperature below 4°C enters the pond and that a gravity underflow, here called a negatively buoyant jet, occurs when water with high total dissolved solids or temperature near 4°C enters the pond and sinks to the bottom of the pond.

The above examples show the importance of considering the characteristics of the in-flow, salt runoff and temperature in the construction of a stormwater detention tank or stormwater pond. The objective of the present study is to investigate how an incoming jet – buoyant, neutrally buoyant or negatively buoyant – affects the residence time and flow pattern in a rectangular tank (13 × 9 × 1 m). While this study concerns temperature differences between the incoming water and tank water, the results of the study would also be applicable to stratification caused by suspended particles or salt. The results of the numerical simulations were compared to physical model tests for a neutrally buoyant jet.

Method

Governing equations

Numerical simulations were made to gain a better understanding of the temperature influence on flow pattern and residence time in the tank. The Fluent (Fluent 2003) commercial CFD (Computational Fluid Dynamics) code was used. The expected complex flow pattern caused by the temperature difference requires simulations in three dimensions. The flow pattern and temperature distribution in the tank was simulated by solving the time-averaged Navier–Stokes equations. For transient flow the continuity equation Equation (1) and momentum equations Equation (2) (Wilcox 1998; Fluent 2003) are expressed:

$$\frac{\partial \rho}{\partial t} + \frac{\partial}{\partial x_i}(\rho U_i) = 0 \tag{1}$$

$$\rho \frac{\partial U_i}{\partial t} + U_j \frac{\partial}{\partial x_j}(\rho U_i) = -\frac{\partial P}{\partial x_i} + \frac{\partial}{\partial x_j}\left[2\mu S_{ji} - \rho\overline{u_i' u_j'}\right] + \rho g_i \tag{2}$$

where U_i = average velocity in the x, y and z directions; u_i' = fluctuating velocity in the x, y and z directions; P = average pressure; x_i = coordinate; μ = molecular dynamic viscosity; S_{ji} = mean strain-rate tensor; ρ = density; t = time and g_i = acceleration of gravity. Since the density of water is temperature-dependent, the buoyancy is also included in the model. The last term in Equation (2) is the gravitational body forces. The term

labelled $-\rho\overline{u_i' u_j'}$ is the Reynolds stress tensor, which represents the turbulence. The Reynolds stress tensor needs to be modelled to close the equation system. There are several different ways of modelling the Reynolds stress term. The classical two-equation standard $k-\varepsilon$ model was used in this study (Launder and Spalding 1974). This is the most widely used turbulence model in engineering applications.

The standard $k-\varepsilon$ model is based on the assumption by Boussinesq that the Reynolds stresses are linked to the velocity gradients via the turbulent dynamic viscosity, μ_t, Equation (3):

$$\tau_{ij} = -\rho\overline{u_i' u_j'} = \mu_t\left(\frac{\partial U_i}{\partial x_j} + \frac{\partial U_j}{\partial x_i}\right). \tag{3}$$

The turbulent dynamic viscosity, μ_t, for the $k-\varepsilon$ model is formulated as in Equation (4), where C_μ is a dimensionless constant. For the standard $k-\varepsilon$ model, C_μ is 0.09:

$$\mu_t = \rho C_\mu \frac{k^2}{\varepsilon}. \tag{4}$$

The turbulence kinetic energy, k, and its rate of dissipation, ε, are obtained from the following transport equations (Wilcox 1998; Fluent 2003):

$$\frac{\partial(\rho k)}{\partial t} + U_j\frac{\partial(\rho k)}{\partial x_j} = \frac{\partial}{\partial x_j}\left[\left(\mu + \frac{\mu_t}{\sigma_k}\right)\frac{\partial k}{\partial x_j}\right] + \tau_{ij}\frac{\partial U_i}{\partial x_j} - \rho\varepsilon + G_b \tag{5}$$

and

$$\frac{\partial(\rho\varepsilon)}{\partial t} + U_j\frac{\partial(\rho\varepsilon)}{\partial x_j} = \frac{\partial}{\partial x_j}\left[\left(\mu + \frac{\mu_t}{\sigma_\varepsilon}\right)\frac{\partial \varepsilon}{\partial x_j}\right] + C_{\varepsilon 1}\frac{\varepsilon}{k}\tau_{ij}\frac{\partial U_i}{\partial x_j} - C_{\varepsilon 2}\rho\frac{\varepsilon^2}{k} \tag{6}$$

with coefficients

$$C_\varepsilon = 1.44, \quad C_{\varepsilon 2} = 1.92, \quad C_\mu = 0.09, \quad \sigma_k = 1.0, \quad \sigma_\varepsilon = 1.3.$$

The last term in Equation (5) is the generation of turbulence due to buoyancy, G_b, expressed as

$$G_b = \beta g_i \frac{\mu_t}{\sigma_t}\frac{\partial T}{\partial x_i} \tag{7}$$

where T = temperature; β = thermal expansion coefficient; and σ_t = turbulent Prandlt number for energy, which is set to 0.85.

The temperature and tracer distribution in the tank is solved using additional equations for energy and tracer transport. The transport equation for energy is

$$\frac{\partial(\rho T)}{\partial t} + \frac{\partial}{\partial x_i}(\rho T U_i) = \frac{\partial \rho}{\partial x_i}\left[\left(\frac{K}{c_p} + \frac{\mu_t}{\sigma_t}\right)\frac{\partial T}{\partial x_i}\right] \tag{8}$$

where c_p = specific heat and K = thermal conductivity. Fluent solves the energy equation in the form of an enthalpy transport equation. The tracer transport is expressed in Equation (9). The tracer is considered conservative and is represented by the local mass fraction, m (Fluent 2003):

$$\frac{\partial(\rho m)}{\partial t} + \frac{\partial}{\partial x_i}(\rho m U_i) = \frac{\partial}{\partial x_i}\left[\left(\rho D_m + \frac{\mu_t}{Sc_t}\right)\frac{\partial m}{\partial x_i}\right]. \tag{9}$$

In turbulent flow, the diffusion depends on both turbulent diffusion and molecular diffusion. In the physical model tests the fluorescent tracer Rhodamine was used. The molecular diffusion coefficient for Rhodamine was not found but is expected to be of the same order of magnitude as that of NaCl. In the simulations the molecular diffusion coefficient, D_m, for Rhodamine was set to 1×10^{-9} m^2/s. As the turbulent diffusion dominates the diffusion

process, the exact value of the molecular diffusion coefficient has only a small influence on the results. The turbulent diffusion coefficient is obtained from the turbulent dynamic viscosity and the turbulent Schmidt number, Sc_t. The value of the turbulent Schmidt number is set to 0.7, which is commonly accepted and is based on measurements of the spread of velocity and mass concentration in turbulent mixing processes. (Daily and Harlemann 1966). Further information on all models can be found in the Fluent User's Guide (Fluent 2003).

The density of water as a function of temperature was implemented in Fluent with a user-defined function defining the density of pure water, ρ, by a standard equation, Equation (10) (UNESCO 1981):

$$\rho = a_0 + a_1 T + a_2 T^2 + a_3 T^3 + a_4 T^4 + a_5 T^5 \tag{10}$$

where T = temperature (°C); $a_0 = 999.842\ 594$; $a_1 = 6.793\ 952 \times 10^{-2}$; $a_2 = -9.095\ 290 \times 10^{-3}$; $a_3 = 1.001\ \ 685 \times 10^{-4}$; $a_4 = -1.120\ \ 083 \times 10^{-6}$ and $a_5 = 6.536\ 332 \times 10^{-9}$.

Model tank and boundary conditions

A simple rectangular geometry was constructed in the laboratory. The advantage of choosing a simple geometry and making physical model tests in the laboratory as compared to using an existing stormwater pond is that it is easier to control the boundary conditions. The physical model tank was rectangular, 13 × 9 × 1 m (Figure 1). The inlet and outlet of the tank were positioned at the middle of the shorter sides. The inlet was a circular pipe with a diameter of 0.23 m, with its crown placed just beneath the water surface, and the outlet was a rectangular weir 0.8 m wide.

The simulation model of the physical model tank is simple and has approximately 144 000 hexahedral cells. The longest side of a cell in the mesh is 0.2 m. The depth of the tank is resolved with 21 cells. To ensure that the numerical predictions include the main features of the flow, it is necessary to select a fine enough mesh to resolve these features. The mesh resolution must also be balanced against computational time. The results of the simulations reported in Adamsson (1999) showed reasonably good agreement with the measurements, suggesting that the used mesh resolution was sufficiently fine to resolve the major flow pattern. No inlet pipe or outflow weir is included in the model. The inlet is modelled as a circular surface with constant velocity. The turbulence intensity of the inlet is set to 1% and the length scale for dissipation to 1 m. The tracer is assumed to have the same properties as water and was added over a period of three seconds at the inlet. The outlet is a rectangular surface with a pressure outlet boundary condition. Simple boundary conditions are used; no-slip was used on the walls and all walls are set as adiabatic for the energy, implying zero heat flux. The top of the tank was in reality a free water surface but is modelled here as a symmetry surface, i.e. no fluid is allowed to pass it and a free-slip condition is set for

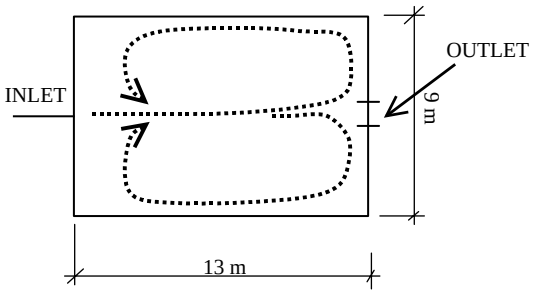

Figure 1 Model tank with major flow pattern for the case with no temperature difference

tangential fluid motion. The vertical displacement of the surface is thus neglected and was in reality small.

Measurements of tracer transport

Tracer measurements were conducted in the physical model tank to compare the simulated tracer transport with the tracer transport in the physical model. A slug of tracer was injected into the inlet pipe approximately 10 m upstream of the inlet of the model tank. The Rhodamine tracer was used, which is a dye with highly fluorescent properties. Lin *et al.* (2003) evaluated the suitability of Rhodamine WT as a tracer for wetland studies and found that it is suitable for small wetland systems where residence times are less than approximately six days and where the sediment contact is limited. A fluorometer was used to continuously measure the tracer concentration at the outlet. The concentrations was measured with a time-averaging of 1–5 s. The intention was to conduct the experiments with the same incoming jet temperature as that in the tank. It was found in the physical model test that it was difficult to fully control the temperature of the inflow water to the tank. Among other things this was because the water was stored in a head tank outside the laboratory building and the water temperature was affected by variations in the outdoor temperature (Adamsson *et al.* 2005). The measurements presented were made in the summer and the expected temperature difference is assumed to be $\Delta T \pm 1$°C.

Simulated cases and simulation procedure

Four different cases were constructed to study how a temperature difference between incoming water and tank water influences the flow pattern and residence time in a detention tank, see Table 1. A negatively buoyant jet is simulated in the first and second cases. In the third a buoyant jet is simulated and in the last case there was no temperature difference between inflow water and tank water. The water in the tank has a temperature of 18°C in Case 1 and the incoming water a temperature of 13°C. In Case 2 the water in the tank has a temperature of 18°C and the incoming water a temperature of 10°C, thus a larger temperature difference. In Case 3 the temperature of the water in the tank is 4°C and the incoming water is 10°C, thus simulating a buoyant jet. This situation may occur in early spring when the pond water is still cold and warm days with a great deal of sun heat the surface runoff. The temperature of the incoming and the tank water is the same in Case 4. All cases have been simulated for three flow rates, 20 l/s, 8 l/s and 4 l/s, which correspond to nominal residence times of 95, 238 and 476 min. The nominal residence time, t_n, is calculated as the tank volume divided by the flow rate. Expressed as surface load, the values range from 610–120 mm/h.

The inflow densimetric Froude number, F_0, is defined as in Gu and Chung (1998) with the difference that the magnitude is used for the density difference. The equation can thus be used for both negatively buoyant and buoyant jets:

Table 1 Cases simulated. The density of pure water for different temperatures was calculated from Equation (10)

					F_0		
	T_{in}	T_{tank}	$\Delta T = T_{in} - T_{tank}$	$\Delta\rho = \rho_{in} - \rho_{tank}$	20 l/s	8 l/s	4 l/s
Case 1	13°C	18°C	−5°C	0.7816 kg/m^3	11.4	4.5	2.3
Case 2	10°C	18°C	−8°C	1.1036 kg/m^3	9.6	3.8	1.9
Case 3	10°C	4°C	+6°C	−0.2729 kg/m^3	19.0	7.5	3.8
Case 4			± 0°C	0 kg/m^3			

$$F_0 = \frac{U_{\text{in}}}{\sqrt{gd\frac{|\rho_{in}-\rho_{\text{tank}}|}{\rho_{\text{tank}}}}} \tag{11}$$

where ρ_{in} = inflow water density; U_{in} = inflow velocity; ρ_{tank} = ambient (tank) water density; g = acceleration of gravity and d = inlet pipe diameter. The densimetric Froude number is a dimensionless number indicating the inertia-to-buoyancy ratio.

The simulation process is divided into two major steps. First the stationary momentum equations are solved and a stationary solution of the flow field is obtained. The stationary flow field serves as the initial condition for the second step. In the second step the heat and tracer transport is modelled, simultaneously solving the momentum equations, the energy transport equations and the tracer transport equations coupled. A coupled simulation is made since the density of water depends on temperature, which will affect the flow pattern. At the start of the transient simulation the tracer is released at the inlet over a period of three seconds and the temperature of the incoming water is simultaneously stepped up or down according to the case simulated. The time step varies from 0.25 s to 30 s and the transient simulation is performed during at least the nominal residence time. Default data are used for most parameters to test that the code can be used as an engineering tool for studying pond hydraulics without previous knowledge of the hydraulic behaviour of the pond studied.

Results and discussion

Simulated residence time distribution curves

Tracer tests are often used to examine the through flow or hydraulic behaviour of ponds and wetlands. The dimensionless impulse response curve of the tracer concentration at the outlet of the tank resulting from an instantaneous injection of tracer at the inlet is referred to as the Residence Time Distribution curve (RTD). The simulated RTDs are shown in Figures 2–4 for 20 l/s, 8 l/s and 4 l/s for the four cases simulated. The dimensionless time is defined as the actual time, t, divided by the nominal residence time, t_n. The dimensionless concentration is the actual concentration, c, divided by a reference concentration, c_0. The reference concentration is defined as the amount of added tracer divided by the tank volume.

An interpretation of the RTDs for 20 l/s shows that the incoming flow travels rapidly to the outlet and that a pulse with high concentrations reaches the outlet at about $0.02t_n$, indicating strong short-circuiting. The residence time of the pulse is thus much lower than the nominal residence time. The difference is small between the case with a buoyant jet and the case with no temperature difference. It is possible to detect a second peak in both these cases when the tracer reaches the outlet after one turn in the tank. For the negatively buoyant jets, the concentration in the peak becomes lower and the peak is wider. For the largest

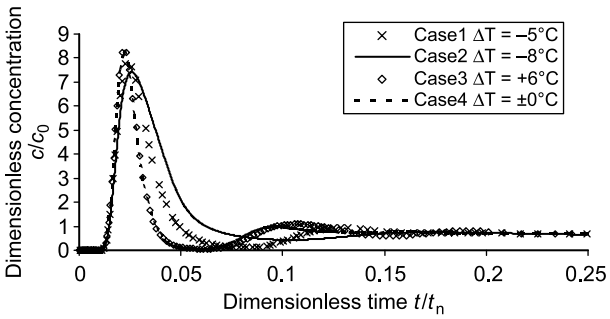

Figure 2 Simulated residence time distribution curve for 20 l/s, Cases 1–4

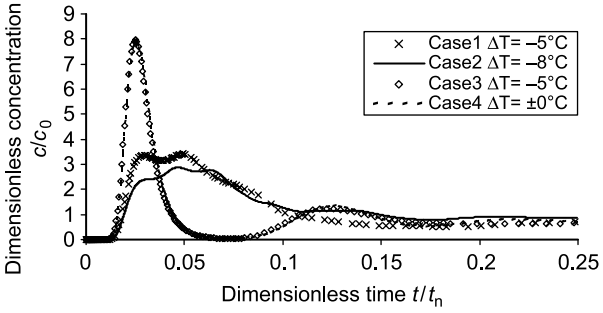

Figure 3 Simulated residence time distribution curve for 8 l/s, Cases 1 – 4

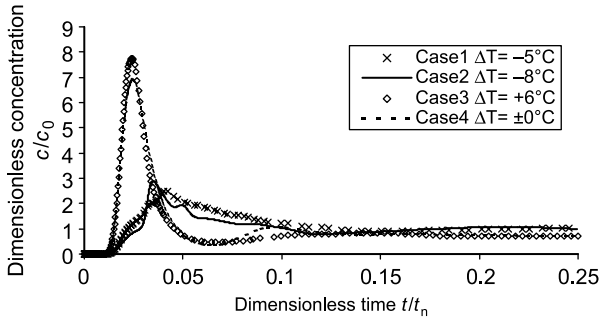

Figure 4 Simulated residence time distribution curve for 4 l/s, Cases 1 – 4

temperature difference, $\Delta T = -8$°C, the second peak is no longer noticeable, which indicates that the gross horizontal circulation in the tank is less apparent.

For the lowest flow rate, 4 l/s, the peak is somewhat higher for the buoyant jet than for the jet with no temperature difference. Still, it arrives rapidly at the outlet. The second peak is not noticeable, which indicates less pronounced circulation. For 8 l/s and 4 l/s the denser inflows give characteristically different RTDs. The first peak is significantly lower and wider, the tracer cloud with highest concentration arrives later at the outlet and the second peak is not noticeable.

Simulated hydraulic parameters

In the literature many different expressions, here called hydraulic parameters, are used as measures of the function of ponds or wetlands, e.g. hydraulic performance, hydraulic efficiency, effective volume, active volume, used volume, short-circuiting, stagnant zones and dead space. All have the purpose of describing how well a pond functions compared to some sort of ideal mode of function or how the pond would generally fulfil its purpose. The shape of the RTD reflects the hydrodynamics of a pond. The RTD represents the time that various fractions of water spend in the pond. Consequently the RTD can be used to calculate a number of hydraulic parameters to evaluate the hydraulic performance. Different hydraulic parameters have been proposed by, for example, Thackston *et al.* (1987), Kadlec and Knight (1996), Ta and Brignal (1998) and Persson *et al.* (1999). A complication is that many different internal flow patterns may result in similar RTDs. This study uses two different measures.

For short-circuiting, measure S proposed by Ta and Brignal (1998) is used, Equation (12). S is a measure of how fast the first part of the tracer arrives compared to the arrival time of the bulk of the tracer. A low value indicates short-circuiting:

$$S = \frac{t_{16}}{t_{50}} \tag{12}$$

Times t_{16} and t_{50} refer to the time from the injection of the tracer pulse until 16% and 50%, respectively, of the injected tracer amount has passed out of the pond. Time t_{16} signifies that the tracer is one standard deviation in advance of the median passage time, t_{50}. Complete plug flow would give $S = 1$, and normally – but not always – a tank exhibiting short-circuiting shows low S values as some tracer is left behind in wakes and eddies, delaying the median passage time.

The effective volume, e, is a measure of how large a fraction of the pond volume partakes in the throughflow, discounting dead zones. Thackston *et al.* (1987) describe dead zones as follows: "dead zones are zones in which velocities toward the outlet are considerable less than average, and in which eddy recirculation currents exist. These zones are not part of the volume through which water flows; thus the effective volume is less than the total volume and the mean residence time is less than the nominal residence time". A high value indicates that a larger part of the volume is in use. The measure for effective volume used in this study is

$$e = \frac{t_{50}}{t_n} \tag{13}$$

This effective volume is a modification of the measure of hydraulic efficiency presented by Thackston *et al.* (1987). In their expression the mean residence time is used instead of the nominal residence time. The simplification has the advantage of not needing to consider the tail of the RTD, which is difficult in practice. The measure of hydraulic efficiency proposed by Thackston *et al.* (1987) was used in the study of Matthews *et al.* (1997). Table 2 shows hydraulic parameters e and S for simulated and measured cases in the present study.

The effective volume, e, and short-circuiting, S, as functions of the densimetric Froude number are shown in Figures 5 and 6.

The simulations show that a somewhat lighter inflow gives the highest effective volume (Figure 5). When a buoyant jet enters the tank, the flow pattern is found to be unstable and the jet has a tendency to wiggle from one side to the other. This makes the fluid more mixed.

Table 2 Hydraulic parameters for simulated and measured cases

Case	Flow rate (l/s)	$e = t_{50}/t_n$	$S = t_{16}/t_{50}$
Case 1 $\Delta T - 5$°C	20	0.65	0.11
Case 2 $\Delta T - 8$°C	20	0.58	0.074
Case 3 $\Delta T + 6$°C	20	0.69	0.18
Case 4 $\Delta T \pm 0$°C	20	0.68	0.18
Physical model test $\Delta T \pm 1$°C	20	0.53	0.10
Case 1 $\Delta T - 5$°C	8	0.58	0.12
Case 2 $\Delta T - 8$°C	8	0.52	0.16
Case 3 $\Delta T + 6$°C	8	0.70	0.18
Case 4 $\Delta T \pm 0$°C	8	0.65	0.19
Physical model test $\Delta T \pm 1$°C	8	0.53	0.18
Case 1 $\Delta T - 5$°C	4	0.53	0.23
Case 2 $\Delta T - 8$°C	4	0.55	0.27
Case 3 $\Delta T + 6$°C	4	0.65	0.17
Case 4 $\Delta T \pm 0$°C	4	0.63	0.16
Physical model test $\Delta T \pm 1$°C	4	0.62	0.09

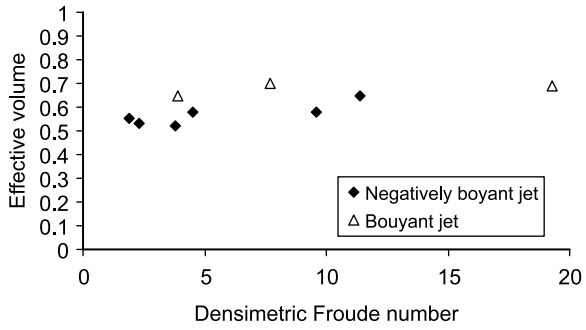

Figure 5 Effective volume, *e*, as a function of densimetric Froude number for simulated Cases 1 – 4

Other general conclusions cannot be drawn from only three simulated buoyant cases. However, it seems that for a buoyant jet in this tank, with the inlet and outlet close to the surface, the influence of Froude number on the effective volume, *e*, and short-circuiting parameter, *S*, is small within the temperature and flow ranges studied.

A denser inflow gives a small decrease in effective volume compared to the neutrally buoyant jet around 10% for low Froude numbers (Table 2). Short-circuiting decreases for negatively buoyant jets at low Froude numbers (Figure 6). The decrease in short-circuiting may be caused by the observed change in flow pattern, from the flow pattern of the neutrally buoyant jet with a surface jet with two large eddies on each side of the jet to the flow pattern of the negatively buoyant jet with a current that travels along the bottom towards the outlet and a counter current at the surface towards the inlet or a stagnant water volume at the surface. The exchange between the bottom and surface layer is small, which will affect the effective volume.

Comparison of the median residence times in the tank shows that, for the densest inflow, 50% of the tracer left the tank after only 56 min (20 l/s), 123 min (8 l/s) and 263 min (4 l/s). The corresponding times for the buoyant jet are 66 min, 166 min and 310 min. Note that the actual median residence times are far from the median residence times in the plug flow case, which are equal to the nominal residence times, 95 min (20 l/s), 238 min (8 l/s) and 476 min (4 l/s).

Comparison between measurements and simulations

The simulations are compared with measurements made for neutrally buoyant jets. Simulated and measured RTDs for the 20 l/s flow rate are shown in Figure 7. The measured RTD has the same shape as the simulated, with a peak with high concentrations and a tail

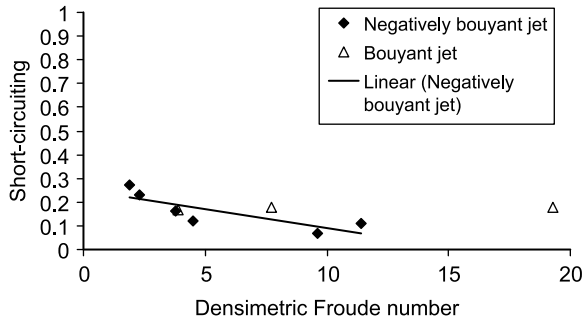

Figure 6 Short-circuiting parameter, *S*, as a function of densimetric Froude number for simulated Cases 1Δ4

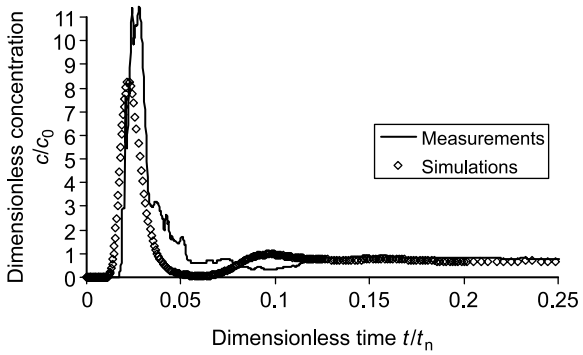

Figure 7 Simulated RTD and measured RTD for 20 l/s

with low concentrations. The time of the first breakthrough is also close. The spreading of the tracer seems stronger in the physical model. The concentration does not reach zero after the first breakthrough, as it does for the simulation before the recirculation. The peak is about 40% higher in the measurements.

A comparison between measured and simulated RTD for the lowest flow rate, 4 l/s, shows large discrepancies (Figure 8). The time required for the tracer to reach the outlet at 4 l/s is much longer in the measurements than in the simulations, implying that the velocities in the jet are higher in the simulation than in the measurements. The peak concentration in the simulations is about half the measured concentration.

Not looking in detail, the large-scale shape of the RTD shows reasonable agreement between measurements and simulations for 20 l/s. However, for 4 l/s, the discrepancies are large.

A comparison of the simulated and measured hydraulic parameters shows that the measurements give a lower effective volume than the simulations (Table 2) for 20 l/s and 8 l/s. Repeated measurements were made, and there is a scatter in calculated effective volume. However, the effective volume calculated from the simulated RTD is most often higher than the measured RTD.

The difference between measured and simulated RTDs can be caused by errors and limitations in the modelling approach for both the measurements and the simulations. During the measurements, the RTDs were found to be sensitive to the background concentration of the Rhodamine tracer. The time lapse between successive measurements may not have been sufficient for the tracer to decay. Mangelson and Watters (1972) found in tracer measurements in waste stabilisation ponds that the RTD was sensitive to eddies and currents

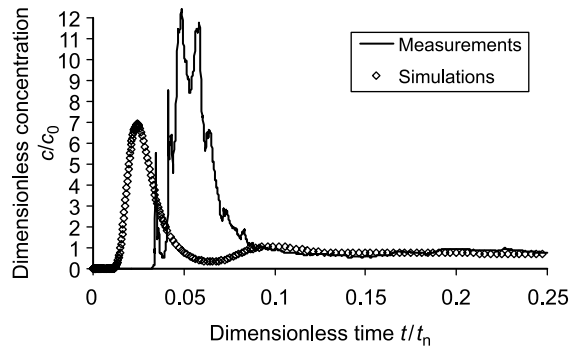

Figure 8 Simulated RTD, 4 l/s, and measured RTD for 4 l/s

that developed during the filling of the model tank. They recommend waiting a certain length of time to allow currents and eddies to die. The same behaviour was found during the start-up of the measurements in the present study. Perhaps the time for developing flow pattern was too short for the low flow rate before the measurements started. Mangelson and Watters (1972) also discuss the random nature of turbulence that affects the tracer flow paths. Other possible sources of error are the calibration of the flow meter and the fluorometer. Further discussion of the tracer measurements can be found in Adamsson *et al.* (2005).

Using simulations always involves assumptions and simplifications. The flow regime in the model tank is indeterminable for low flow rates. The calculated Reynolds number in the tank studied, assuming a water depth and mean velocity based on plug flow, varied between 400 and 2200. Assuming that the jet in the tank is on average 2 m wide and 1 m deep will give a Reynolds number between 2000 and 10 000. For free surface flow, the transition from laminar to turbulent flow is assumed to be around a Reynolds number of 500 to 600. The transition region is generally assumed to be between 500 and 2000 (Chow 1959). According to Chow (1959), the flow regime for 4 l/s is most probably in the transition region. Quarini *et al.* (1996) had similar difficulties modelling flow at low velocities with the standard $k-\varepsilon$ turbulence model. Quarini *et al.* (1996) wrote: "It is well known that the $k-\varepsilon$ turbulence model is poor in the region of low flow and inadequate where the mean velocity gradients go to zero, as occurs in this region of the tank." They studied the hydrodynamic characteristics of a circular sedimentation tank. Another cause of the discrepancies between measurements and simulations may be the way the simulations were done. The temperature was changed at the same time as the tracer was added. The tracer and incoming cold water will be mixed with the warm tank water, and the effect of the colder temperature will be small for the first part of the tracer, which, for example, will have an impact on the time when the initial concentration reaches the outlet.

In the present study it was not possible to determine whether the discrepancies for low flow velocities are due to an insufficient quality of the laboratory measurements or to difficulties in the simulations of the flow in the tank, which is in the transition region.

Flow pattern and tracer transport

Previous studies of the model tank (Adamsson 1999) solved the stationary flow field. For a stationary simulation, the flow pattern in the tank is characterised by a central jet with two eddies, one on each side of the jet. The pattern is similar through the depth of the tank. In the present study transient simulations were made. These simulations show that the incoming jet fluctuates from one side to the other for higher flow rates so that the eddy on one side is alternately larger or smaller than the eddy on the other. A negatively buoyant jet seems to stabilise the flow pattern. Especially for 20 l/s, the fluctuation is not as strong for the negatively buoyant jet as it is for the buoyant jet and the case with no temperature difference.

An advantage of using simulations is that it is possible to visualise the tracer transport at any time, at almost any place in the tank, and at low concentrations. A horizontal view of the tracer transport in the tank reflects the flow pattern in the tank. The pattern of tracer transport is similar for all flow rates for buoyant and neutrally buoyant jets. As examples, horizontal cuts of tracer "clouds" 0.15 m below the surface are shown for a buoyant jet and a negatively buoyant jet. The level of 0.15 m is the same as the level of the centre of the inlet pipe. Figure 9 shows a buoyant case with the flow rate 8 l/s and $\Delta T + 6$°C. The gross circulation of tracer in two almost symmetric eddies around the centre line is distinct. Figure 10 shows a case with a negatively buoyant jet and $\Delta T - 5$°C. Distinct recirculation does not occur in this case. Similar flow patterns occur for all simulated flow cases with a flow rate 8 l/s or smaller. The concentration is amplified between the figures. The inlet is to the left in all figures.

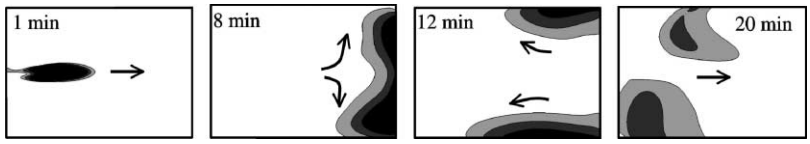

Figure 9 Tracer cloud for $\Delta T + 6$°C, 8 l/s

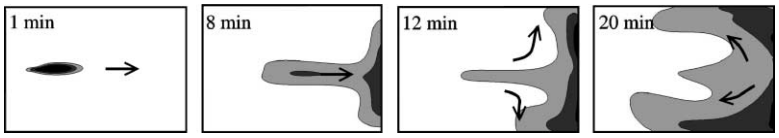

Figure 10 Tracer cloud for $\Delta T - 5$°C, 8 l/s

As mentioned earlier, negatively buoyant jets with low Froude numbers sink towards the bottom and travel along the bottom to the outlet. For ponds and tanks with surface inflow there would exist a critical Froude number below which the negatively buoyant jet is affected by gravity and the flow exhibits a bottom current and above which the flow pattern is the same as for a neutrally buoyant jet. The flow pattern was plotted for the different simulated cases and, within the studied range of temperatures and flow rates, the flow pattern was observed to change for a flow rate of 8 l/s and a negatively buoyant jet Froude number of 3–5. This can also be observed in Figure 6: the short-circuiting parameter increased when the flow pattern changed from a surface jet to a bottom current. In Figure 11 vertical, longitudinal sections of tracer concentration in the tank are shown after 1, 2 and 6 min for a buoyant jet. The tracer is transported and has the highest concentrations close to the surface. Figure 12 shows the tracer transport for a denser inflow is shown. The highest concentration here is transported along the bottom of the tank. The sections are taken from the centre of the inlet to the outlet.

There are both positive and negative consequences of a negatively buoyant jet. The bottom current can cause erosion of sediment resulting from increased bottom velocities. An advantage may be that the bottom currents increase the oxygenation at the bottom and prevent the formation of a bottom zone with anaerobic conditions.

When the tracer cloud is transported from the inlet towards the outlet, the tracer will be diluted owing to diffusion. The dilution of the tracer is illustrated in Figure 13. The tracer concentration along a line from the centre of the inlet pipe to the outlet is plotted after 1, 2 and 4 min for a flow rate of 8 l/s for a buoyant and a negatively buoyant jet. The tracer

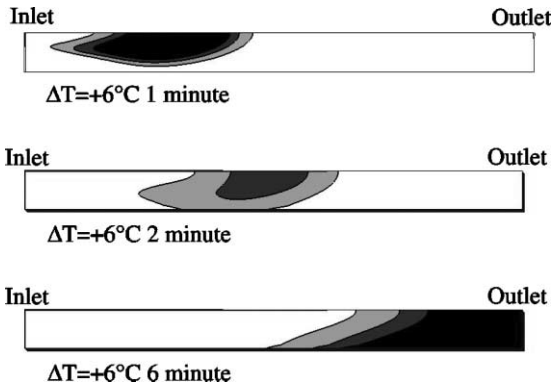

Figure 11 Tracer transport along the centre of the tank, $\Delta T = +6$°C, flow rate 8 l/s

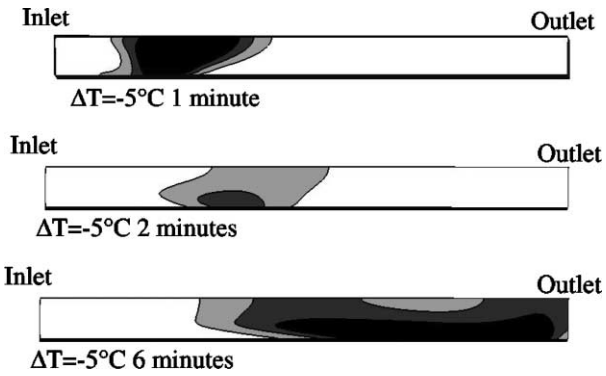

Figure 12 Tracer transport along the centre of the tank, $\Delta T = -5$°C, flow rate 8 l/s

concentration was 10% of the amount of the inflow rate. After just one minute in the tank the tracer is diluted about 50 times for the buoyant jet and 100 times for the negatively buoyant jet. Even though the negatively buoyant jet is more diluted, the negatively buoyant jet gives a smaller effective volume than the buoyant jet. This is caused by the flow pattern with two layers, one stagnant layer with low flow velocities at the surface and a bottom current towards the outlet, which will act to reduce the mixing processes in the tank and decrease the effective volume.

A large dilution or dispersion can be advantageous, for example after a heavy storm when highly polluted water enters a pond or an accident causes unwanted pollutants to enter the pond. The immediate toxicity will be less with greater dilution.

Denser inflow caused by salt

In the literature review references were found that reported increased salinity in snow melt water. The results and conclusions in this study could also be applied to stratifications caused by salt and suspended solids. Mayer *et al.* (2000) measured the conductivity throughout the depth of a detention pond in Canada. The conductivity measured at the surface was 1.65 mS/cm, and close to the bottom, at a depth of 4 m, it was 9 mS/cm. Pettersson (1999) measured conductivities in the effluent water from a stormwater pond during winter. The specific conductivity was around 1 mS/cm at an event in November and increased to 10 mS/cm during a snowmelt event in February. Pettersson derived the high specific conductivity to road salting. The temperature in the pond was more or less constant around +4°C during this period. The conductivity and stratification within the pond was not measured however. Assume that the conductivity in the pond is unchanged over the winter, around 1mS/cm, and at the first snowmelt event the incoming conductivity will be around 10 mS/cm. Translating these conductivities to density difference would give $\Delta\rho = 3$–$4\,\mathrm{kg/m^3}$, which is about three

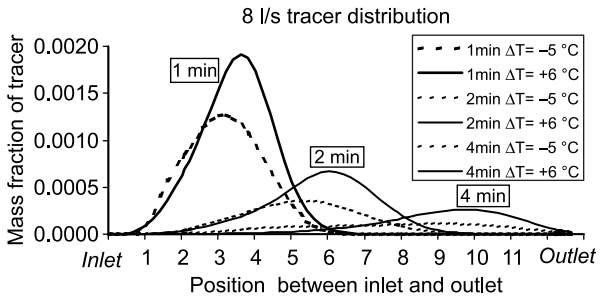

Figure 13 Tracer concentration along a line from the centre of the inlet to the outlet for the flow rate 8 l/s

times as large as the density differences simulated in this study. The impact of salt on water density is much larger than that of temperature.

Conclusions

The effect of a buoyant or negatively buoyant jet on residence time and flow pattern in a rectangular detention tank has been investigated using three-dimensional simulations. There are limitations in the simulation approach, but the following conclusions are reasonable.

The results show that a buoyant jet gives a higher effective volume than a negatively buoyant jet for a tank with an inlet close to the surface. For a buoyant or neutrally buoyant jet, the influence of densimetric Froude number on short-circuiting and effective volume is small, and the flow pattern is characterised by a central jet with two large eddies, one on each side of the jet.

A negatively buoyant jet gives less effective volume than a neutrally buoyant jet, and a negatively buoyant jet, with low densimetric Froude number, decreases short-circuiting in the tank. One reason for the decrease in short-circuiting can be the change in flow pattern with a bottom current and an either stagnant water body at the surface or a counter current at the surface towards the inlet. The exchange between the surface water and the bottom water is small and will probably decrease the effective volume.

Comparison between simulated and measured RTDs shows reasonable agreement for high flow rates. For low flow rates, the discrepancies between measurements and simulations are large, possibly due to both insufficient quality of the laboratory experiments and limitations in the numerical simulation approach, for example inadequate turbulence modelling for low-momentum jets of small discharge into large volumes of water. It is further shown that three-dimensional simulations would be useful when studying flow pattern and temperature distribution in a tank. The simulations with negatively buoyant jets and low densimetric Froude numbers show a typical three-dimensional flow pattern, which means that, to be able to capture the flow behaviour, simulations in three dimensions are needed.

The study also shows the importance of considering inflow boundary conditions such as temperature and salinity when studying the performance of detention tanks and stormwater ponds. Even though the water depth in the model was only 1 m, stratification occurred for low flow rates. In real circumstances the effect of wind must be taken into account. The literature indicates that measured density differences as large as 3–4 kg/m^3 due to salt concentration in stormwater ponds is possible. This is about three times as large as the density differences simulated in this study. The impact of salt on density is large, and stratification during spring and winter conditions due to road salting in stormwater ponds is therefore very probable. As shown in this paper, both the effective volume and the flow pattern may be affected.

Acknowledgement

The Swedish Council for Building Research (BFR) is gratefully acknowledged for financial support.

References

Adamsson, Å. (1999). Computational fluid dynamics for detention tanks, simulation of flow pattern and sedimentation. Licentiate thesis, Dept. of Hydraulics, Chalmers University of Technology, Göteborg, Sweden.

Adamsson, Å., Bergdahl, L. and Lyngfelt, S. (2005). Measurement and three-dimensional simulation of flow in a rectangular detention tank. *Urban Water Journal*, **2**(4), 277–287.

Chow, V.T. (1959). *Open-channel Hydraulics*. McGraw-Hill, Tokyo.

Daily, J.W. and Harleman, D.R.F. (1966). *Fluid Dynamics*. Addison-Wesley, Reading, MA.

Fluent (2003). *Fluent 6.1, User's Guide*, Fluent Inc., Lebanon, NH.

German, J. (2003). Reducing stormwater pollution, performance of retention ponds and street sweeping. PhD thesis, Dept. of Water Environment Transport, Chalmers University of Technology, Göteborg, Sweden.

German, J., Svensson, G., Gustafsson, L.-G. and Vikström, M. (2003). Modelling of temperature effects on removal efficiency and dissolved oxygen concentrations in stormwater ponds. *Wat. Sci. Technol.*, **48**(9), 145–154.

Gu, R. and Chung, S.-W. (1998). Reservoir flow sensitivity to inflow and ambient parameters. *J. Wat. Res. Planning Mngmnt.*, **123**(3), 119–128.

Hvitved-Jacobsen, T., Johansen, N.B. and Yousef, Y.A. (1994). Treatment systems for urban and highway run-off in Denmark. *Sci. Total Environ.*, **146/147**, 499–506.

Kadlec, R. and Knight, R. (1996). *Treatment Wetlands*. Lewis Publishers, Boca Raton, FL.

Larm, T. (2000). Watershed-based design of stormwater treatment facilities: model development and applications. PhD thesis, Dept. of Civil and Environmental Engineering, Royal Institute of Technology, Stockholm, Sweden.

Launder, B.E. and Spalding, D.B. (1974). The numerical computation of turbulent flows. *Comput. Meth. Appl. Mech. Engng.*, **3**, 269–289.

Lin, A.Y.-C., Debroux, J.-F., Cunningham, J.A. and Reinard, M. (2003). Comparison of rhodamine WT and bromide in the determination of hydraulic characteristics of constructed wetlands. *Ecol. Engng.*, **20**, 75–88.

Mangelson, K.A. and Watters, G.Z. (1972). Treatment efficiency of waste stabilization ponds. *J. Sanitary Engng. Div., ASCE SA2*, **98**, 407–425.

Marsalek, P.M., Watt, W.E., Marsalek, J. and Anderson, B.C. (2000). Winter flow dynamics of an on-stream stormwater management pond. *Wat. Qual. Res. J. Can.*, **35**(3), 505–523.

Marsalek, P.M., Watt, W.E., Marsalek, J. and Anderson, B.C. (2003). Winter operation of an on-stream stormwater management pond. *Water Science and Technology*, **48**(9), 133–143.

Matthews, R.R., Watt, W.E., Marsalek, J., Crowder, A.A. and Anderson, B.C. (1997). Extending retention times in a stormwater pond with retrofitted baffles. *Wat Qual. Res. J. Can.*, **32**(1), 73–87.

Mayer, T., Rochfort, Q. and Borgmann, U. (2000). Impact of road salts on small urban ponds: Rouge river pond case study. In J. Pries (ed.), *Treatment wetlands for water quality improvement*, Proceedings of the Millennium Wetland Event, Quebec City, Canada, August 6–12, 2000. pp. 211–217.

Oberts, G. (1994). Performance of stormwater ponds and wetlands in winter. *Watershed Prot. Tech.*, **1**(2), 55–61.

Oberts, G., Marsalek, J. and Viklander, M. (2000). Review of water quality impacts of winter operation of urban drainage. *Wat. Qual. Res. J. Can.*, **35**(4), 781–808.

Persson, J. (2000). The hydraulic performance of ponds of various layouts. *Urban Wat.*, **2**(3), 243–250.

Persson, J., Somes, N.L.G. and Wong, T.H.F. (1999). Hydraulics efficiency of constructed wetlands and ponds. *Wat Sci. Technol.*, **40**(3), 291–300.

Pettersson, T.J.R. (1999). The effects of variations of water quality on the partitioning of heavy metals in a stormwater pond. In I.B. Joliffe and E.B. Ball (eds), *Proc. 8th Int. Conf. on Urban Storm Drainage*, 30 Aug. – 3 Sep., 1999, Sydney, Australia, vol 4. The Institution of Engineers, Australia, 1943–1946.

Quarini, G., Innes, H., Smith, M. and Wise, D. (1996). Hydrodynamic modelling of sedimentation tanks. *Proc. Inst. Mech. Engrs.*, **210**, 83–91.

Shaw, J.K.E., Watt, W.E., Marsalek, J., Anderson, B.C. and Crowder, A.A. (1997). Flow pattern characterization in urban stormwater detention pond and implications for water quality. *Wat. Qual. Res. J. Can.*, **32**(1), 53–71.

Ta, C.T. and Brignal, W.J. (1998). Application of computational fluid dynamics technique to storage reservoir studies. *Wat. Sci. Technol.*, **37**(2), 219–226.

Thackston, E.L., Shields, F.D. and Schroeder, P.R. (1987). Residence time distributions of shallow basins. *J. Environ. Engng.*, **113**(6), 1319–1332.

UNESCO (1981). *Tenth Report of the Joint Panel on Oceanographic Tables and Standards*, UNESCO technical papers in marine science 36, Sidney, BC, Canada.

Van Buren, M.A., Watt, W.E., Marsalek, J. and Anderson, B.C. (2000). Thermal balance of on-stream storm-water management pond. *J. Environ. Engng.*, **126**(6), 509–517.

Walker, D.J. (1998). Modelling residence time in stormwater ponds. *Ecol. Engng.*, **10**, 247–262.

Wilcox, D.C. (1998). *Turbulence Modeling for CFD*. DCW Industries, Inc., La Cañada, CA, USA.